Bi-allelic expression of the RyR1 p.A4329D mutation decreases muscle strength in slow-twitch muscles in mice

Received for publication, April 11, 2020, and in revised form, May 29, 2020 Published, Papers in Press, June 4, 2020, DOI 10.1074/jbc.RA120.013846

Moran Elbaz[1,‡], Alexis Ruiz[1,‡], Sven Nicolay[1], Chiara Tupini[2], Christoph Bachmann[1], Jan Eckhardt[1], Sofia Benucci[1], Pawel Pelczar[3], Susan Treves[1,2], and Francesco Zorzato[1,2,*]

From the [1]Department of Biomedicine, Basel University Hospital, Basel, Switzerland, [2]Department of Life Science and Biotechnology, University of Ferrara, Ferrara, Italy, and [3]Center for Transgenic Models, University of Basel, Basel, Switzerland

Mutations in the ryanodine receptor 1 (*RYR1*) gene are associated with several human congenital myopathies, including the dominantly inherited central core disease and exercise-induced rhabdomyolysis, and the more severe recessive phenotypes, including multiminicore disease, centronuclear myopathy, and congenital fiber type disproportion. Within the latter group, those carrying a hypomorphic mutation in one allele and a missense mutation in the other are the most severely affected. Because of nonsense-mediated decay, most hypomorphic alleles are not expressed, resulting in homozygous expression of the missense mutation allele. This should result in 50% reduced expression of the ryanodine receptor in skeletal muscle, but its observed content is even lower. To study in more detail the biochemistry and pathophysiology of recessive *RYR1* myopathies, here we investigated a mouse model we recently generated by analyzing the effect of bi-allelic *versus* mono-allelic expression of the RyR1 p.A4329D mutation. Our results revealed that the expression of two alleles carrying the same mutation or of one allele with the mutation in combination with a hypomorphic allele does not result in functionally equal outcomes and impacts skeletal muscles differently. In particular, the bi-allelic RyR1 p.A4329D mutation caused a milder phenotype than its mono-allelic expression, leading to changes in the biochemical properties and physiological function only of slow-twitch muscles and largely sparing fast-twitch muscles. In summary, bi-allelic expression of the RyR1 p.A4329D mutation phenotypically differs from mono-allelic expression of this mutation in a compound heterozygous carrier.

Muscle contraction is brought about by a massive release of Ca^{2+} from the sarcoplasmic reticulum (SR) throughout the entire length of the muscle fiber via a process called excitation-contraction coupling (ECC) (1, 2). Calcium release from the SR via the calcium release channel ryanodine receptor is initiated by a voltage-dependent orthograde signal delivered by the dihydropyridine receptor (DHPR), the voltage sensor localized in the transverse tubule membrane (T-tubules). Muscle relaxation is brought about by calcium reuptake into the SR by the sarco (endo)plasmic CaATPase (SERCA). ECC occurs at the contact region between the T-tubules and the SR membrane, within a domain encompassing a macromolecular complex formed by the ryanodine receptor 1 (RyR1), DHPR, and the calcium-buffering protein calsequestrin (3–5).

Mutations in *RYR1*, the gene encoding RyR1, have been identified in patients with a variety of neuromuscular disorders (6–8), including malignant hyperthermia susceptibility (MIM number 145600) (9), central core disease (CCD; MIM number 11700) (10), specific forms of multiminicore disease (MmD; MIM number 255320) (11), centronuclear myopathy (CNM; MIM number 255320), and congenital fiber type disproportion (12). A great deal of data has shown that recessive *RYR1* mutations are mostly linked to cases of MmD, CNM, or congenital fiber type disproportion; patients with recessive mutations may carry homozygous mutations (*i.e.* the same mutation in both alleles) or two different mutations, one inherited from the paternal allele and the other from the maternal allele. In many patients carrying compound heterozygous mutations, one of the mutations causes a premature termination of the RyR1 protomer, leading to the mono-allelic and homozygous expression of a missense mutation. One of the molecular signatures of the mono-allelic expression of a missense mutation is a dramatic decrease of the RyR1 protein content in total muscle homogenates from patients and the overexpression of chromatin-modifying enzymes, such as histone deacetylases (HDACs) and DNA methyltransferases (DNMTs) (13).

We have recently developed a mouse model carrying compound heterozygous recessive *Ryr1* mutations isogenic with those identified in severely affected MmD patients (14), namely, the frameshift RyR1 p.Q1970fsX16 mutation in exon 36 plus the missense mutation RyR1 p.A4329D in exon 91. The focus of this study is to determine whether phenotypic differences result from the presence of a homozygous *Ryr1* mutation and the mono-allelic expression of the same *Ryr1* mutation on the genetic background of a compound heterozygous carrier (with the other allele carrying a null mutation). In particular, in the present report we have examined the phenotype of mice carrying the homozygous mutation in *Ryr1* exon 91 (referred to as HO91) compared with that of the mouse model carrying the compound heterozygous mutation in exon 36 and exon 91 (15) (referred to as DKI) and that of a mouse heterozygous for the expression of the exon 91 mutation (referred to as Het91). Our results show that at variance with compound heterozygous RyR1Q1970fsX16+A4329D mice, the homozygous expression of the RyR1 p.A4329D mutation (referred to as RyR1A4329D mice) mainly affects slow-twitch muscles, with negligible effects on fast-twitch muscles. In particular, our results show

This article contains supporting information.
‡These authors contributed equally to this work.
*For correspondence: Francesco Zorzato, zor@unife.it; fzorzato@usb.ch.

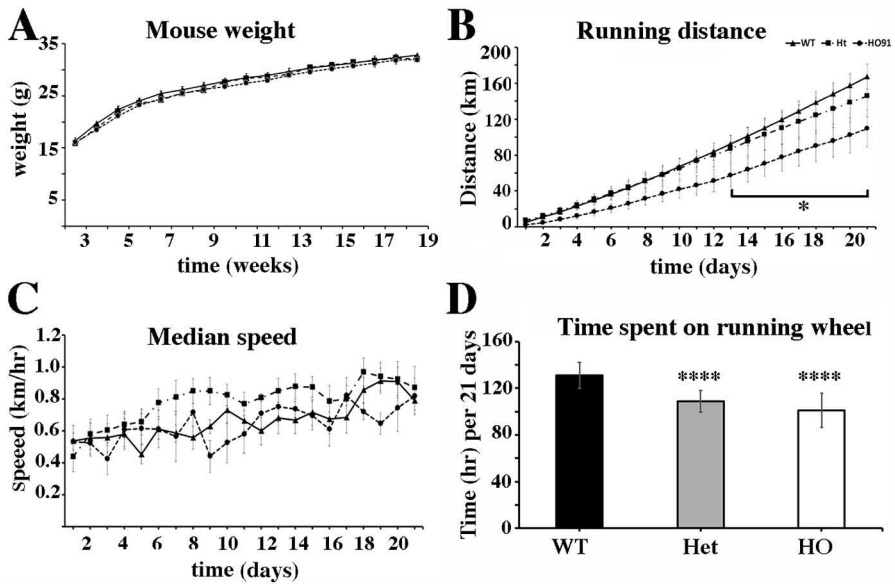

Figure 1. Body weight and *in vivo* muscle function of homozygous and heterozygous RyR1A4329D male mice. *A*, the body weight gain over a period of 18 weeks is similar in WT ($n = 12$), Het91 ($n = 11$), and HO91 mice ($n = 10$). *B* and *C*, total running distance (*B*) and total running speed (*C*) of WT, Het91, and HO91 male mice. Spontaneous running activity was measured for 21 days in individually housed 12-week-old WT ($n = 12$; *filled triangles*, *continuous line*), Het91 ($n = 8$; *filled squares*, *dash-dotted line*), and HO91 ($n = 7$; *filled circles*, *dashed line*) mice during the dark phase. Each cage was equipped with a running wheel. Each symbol represents the mean (±S.E.). $p \leq 0.05$ (Mann-Whitney two-tailed test). *D*, calculated mean (±S.E.) time spent on the running wheel over 21 days (WT, $n = 12$; Het91, $n = 8$; HO91, $n = 7$). $p < 0.0001$ (Mann-Whitney two tailed test).

that the homozygous expression of RyR1 p.A4329D causes a decrease of the RyR1 protein content in total muscle homogenates from soleus muscles only. The reduction of RyR1 protein is associated with a decrease of the (i) total running distance, (ii) the peak twitch and tetanic force in soleus muscles, and (iii) the peak twitch and tetanic calcium transient in soleus muscles.

Results

In vivo phenotype of homozygous and heterozygous RyR1A4329D mice

The presence of the homozygous missense mutation in *Ryr1* Ex91 of the mice used for the experiments was confirmed by diagnostic digestion of PCR-amplified DNA with the restriction enzyme PvuII (Fig. S1). RyR1A4329D homozygous (HO91) mice did not exhibit a postnatal lethal phenotype or defects in embryonic development and were indistinguishable from WT or Het91 *Ryr1* mutant carrier littermates. Analysis of the growth curves performed during the observation period of 18 weeks indicates that both male and female HO91 mice exhibit a body weight similar to that of WT littermates (Fig. 1*A*). The growth curve of Het91 mice was similar to that of their WT littermates.

The presence of the homozygous RyR1 p.A4329D mutation functionally impacts in vivo muscle function in mice

We used the voluntary running wheel setup (16) to investigate the *in vivo* skeletal muscle function of RyR1A4329D mutant mice. Mice had free access to the running wheel at any time of day; this experimental approach avoids potential problems linked to the effect of circadian rhythm on animal activity and/or animal compliance in performing nonvoluntary motor activity. The total dark phase running distance of three-month-old HO91 and Het91 mice was compared with that of their WT littermates (Fig. 1*B*). In the first week, the total running distance of WT and mutant mice was similar. 2 weeks of training improved skeletal muscle performance in all groups. After 3 weeks of training, the total running distance of the WT and Het91 mice was ~34% longer than that of HO91 mice (Mann-Whitney two-tailed test, calculated over the running period of 21 days; $p < 0.05$, $n = 12$ WT, $n = 8$ heterozygous, and $n = 7$ homozygous). The shorter running distance was also associated with a lower median cruise speed of the HO91 mutant mice than WT littermates (Fig. 1*C*; $p < 0.05$ by Mann-Whitney test, two-tailed test). Interestingly, both HO91 and Het91 mice spent significantly less time on the running wheel than their WT littermates (Fig. 1*D*).

The homozygous RyR1 p.A4329D mutation decreases isometric force development only in soleus muscles

The reduced speed and shorter total running distance of the HO91 mice may result from reduced muscle strength caused by alterations of the macromolecular complexes involved in ECC. We examined such a possibility by investigating the mechanical properties of intact *extensor digitorum longus* (EDL) and soleus muscles upon delivery of a single action potential or by a train of pulses of 1.0-ms duration delivered at 50, 100, and 150 Hz for 400 ms in EDL muscles and at 50, 100, and 120 Hz for 1100 ms in soleus muscles (Fig. 2) (16). The averaged specific twitch peak force induced by a single action potential in EDL from HO91 mice was similar to that of EDL from WT mice (Fig. 2) (72.07 ± 12.52 mN/mm^2, $n = 9$, *versus* 86.44 ± 25.05 mN/mm^2, $n = 11$, respectively; values are expressed as mean ± S.D., $p < 0.05$). Similarly, the specific tetanic force was similar in EDL from WT and HO91 mice (360.34 ± 64.17 mN/mm^2, $n = 11$, *versus* 337.55 ± 35.09 mN/

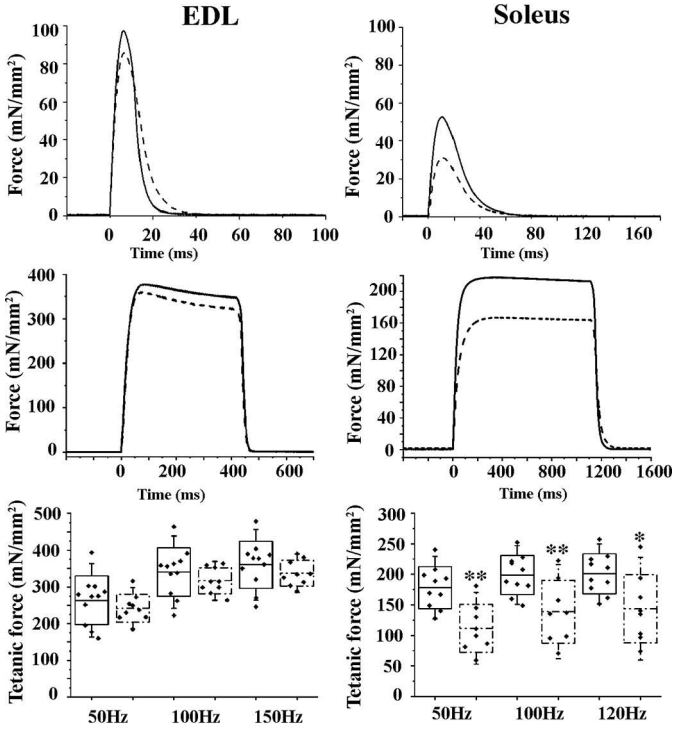

Figure 2. Mechanical properties of EDL and soleus muscles from WT and HO91 mice. *Top*, representative traces of single twitches. *Central*, representative traces of maximal tetanic forces in EDL and soleus muscles. WT, *continuous line*; *dashed line*, HO91. *Bottom*, whisker plots of tetanic force generated by isolated muscles from WT and HO91 mice electrically stimulated at 50 Hz, 100 Hz, and 150 Hz (EDL muscles) and electrically stimulated at 50 Hz, 100 Hz, and 120 Hz (soleus muscles). Each symbol represents the value from a single mouse: WT EDL, $n = 11$; HO91 EDL, $n = 9$; WT soleus, $n = 10$; HO91 soleus, $n = 8$. **, $p \leq 0.01$ (Mann-Whitney two-tailed test).

mm^2, $n = 9$, respectively; values are expressed as mean ± S.D., $p < 0.05$). On the other hand, soleus muscles from HO91 mice exhibited a 36% decrease of twitch specific peak force compared with that of WT littermates (34.20 ± 15.57 mN/mm^2, $n = 9$, *versus* 52.75 ± 11.15 mN/mm^2, $n = 10$, respectively; values are expressed as mean ± S.D.; $p < 0.05$), as well as a 30% decrease in the maximal specific tetanic force (200.72 ± 32.82 mN/mm^2, $n = 10$, *versus* 143.66 ± 55.96 mN/mm^2, $n = 8$, in WT and HO91, respectively; values are expressed as mean ± S.D., $p < 0.05$). The specific force (twitch and tetanic) of EDL and soleus muscles from the Het91 mice were not different from those of littermate WT mice (Fig. S2).

The decrease in force output cannot be accounted for by fast-to-slow fiber transition, because there were no changes in the expression of myosin heavy-chain (MyHC) isoforms in EDL and soleus muscles (Fig. 3*A* and *B*). Similarly, the reduced absolute force developed cannot be attributed to a major loss of contractile proteins, as the wet weight of the EDL and soleus muscles from HO91 and WT mice were similar (muscle wet weight of EDL was 12.79 ± 1.54 mg, $n = 11$, *versus* 11.21 ± 1.10 mg, $n = 9$, in WT and HO91 mice, respectively). Values are expressed as mean ± S.D., $p < 0.05$. Wet weight of soleus was 12.37 ± 2.06 mg, $n = 10$, *versus* 12.16 ± 0.93 mg, $n = 9$, in WT and HO91, respectively; values are expressed as mean ± S.D., $p > 0.05$. On the other hand, soleus muscles from HO91 mice show a small decrease of the minimal Feret's fiber diameter, indicating a slight atrophy of the slow-twitch fibers (Fig. 3*A*, *C*, and *D*), which may explain, at least in part, the decrease of muscle strength. No histological changes were present in EDL and soleus muscles from Het91 mice (results not shown).

The homozygous RyR1 p.A4329D mutation decreases RyR1 and $Ca_v1.1$ content in sarcotubular membranes from slow-twitch muscles

The decreased muscle strength of RyR1A4329D mice was apparently not because of fast-to-slow fiber type transition but rather may be linked to atrophy of slow-twitch muscles, to alterations of the expression of ECC components, or to a combination of both. Thus, we investigated the protein content and transcripts encoding the major protein components of the macromolecular complex involved in skeletal muscle ECC (17). Transcript quantification was assessed by real-time quantitative PCR (qPCR) comparing WT and HO91 samples. No changes in the expression levels of Cacna1s, Stac3, and Ryr1 transcripts were apparent in EDL and soleus muscles from HO91 mice (Fig. 4*A*). We also investigated if the levels of histone deacetylases as class II HDACs are elevated in muscles of patients carrying recessive *RYR1* mutations (13) as well as in the DKI mice (15). The expression of Hdac9 (a class IIa deacetylase) was elevated in soleus muscles from HO91 mice, whereas the levels of expression of the other HDACs were similar in WT and HO91 muscles (Fig. 4*A*). The contents of the main protein components of sarcotubular membranes in total homogenate from EDL and soleus muscles from WT and HO91 mice were determined by quantitative Western blot analysis. Figure S3 shows the specific immunoreactivity of the antibodies that were used for Western blot analysis. No significant changes in $Ca_v1.1$, RyR1, Stac3, SERCA1, SERCA2, calsequestrin, calreticulin, and JP45 protein content were observed in EDL total homogenates from HO91 mice (Fig. 4*B*). Interestingly, however, RyR1 and $Ca_v1.1$ protein content was significantly reduced in soleus muscles from HO91 mice compared with that of WT littermates (RyR1 content was 64.0 ± 19.8% of WT [mean ± S.E.], $n = 13$, $p < 0.01$, and $Ca_v1.1$ content was 44.9 ± 7.9% of WT [mean ± S.E.], $n = 7$, $p < 0.05$). The content of the other SR proteins analyzed was unchanged (Fig. 4*B*). ECC protein content was unaltered in muscles from Het91 mice (results not shown).

The decrease of RyR1 and $Ca_v1.1$ observed in soleus muscles should affect the amount of calcium released during ECC, and this was directly investigated by measuring calcium transients in single EDL and soleus fibers loaded with the low-affinity calcium indicator MagFluo4.

Calcium transients in isolated EDL and soleus fibers from WT and RyRA4329D mice

The resting calcium concentration ($[Ca^{2+}]_i$) was measured with the ratiometric Ca^{2+} indicator Fura-2, and there were no differences between EDL and soleus fibers from HO91 and WT mice (Fig. 5*A*). In line with previous results (18), the resting $[Ca^{2+}]_i$ of soleus fibers was higher than that of EDL fibers. In particular, the mean ± S.E. resting $[Ca^{2+}]_i$ in soleus was 86.5 ± 6.3 nM ($n = 29$) and 82.3 ± 4.5 nM ($n = 29$), and in EDL

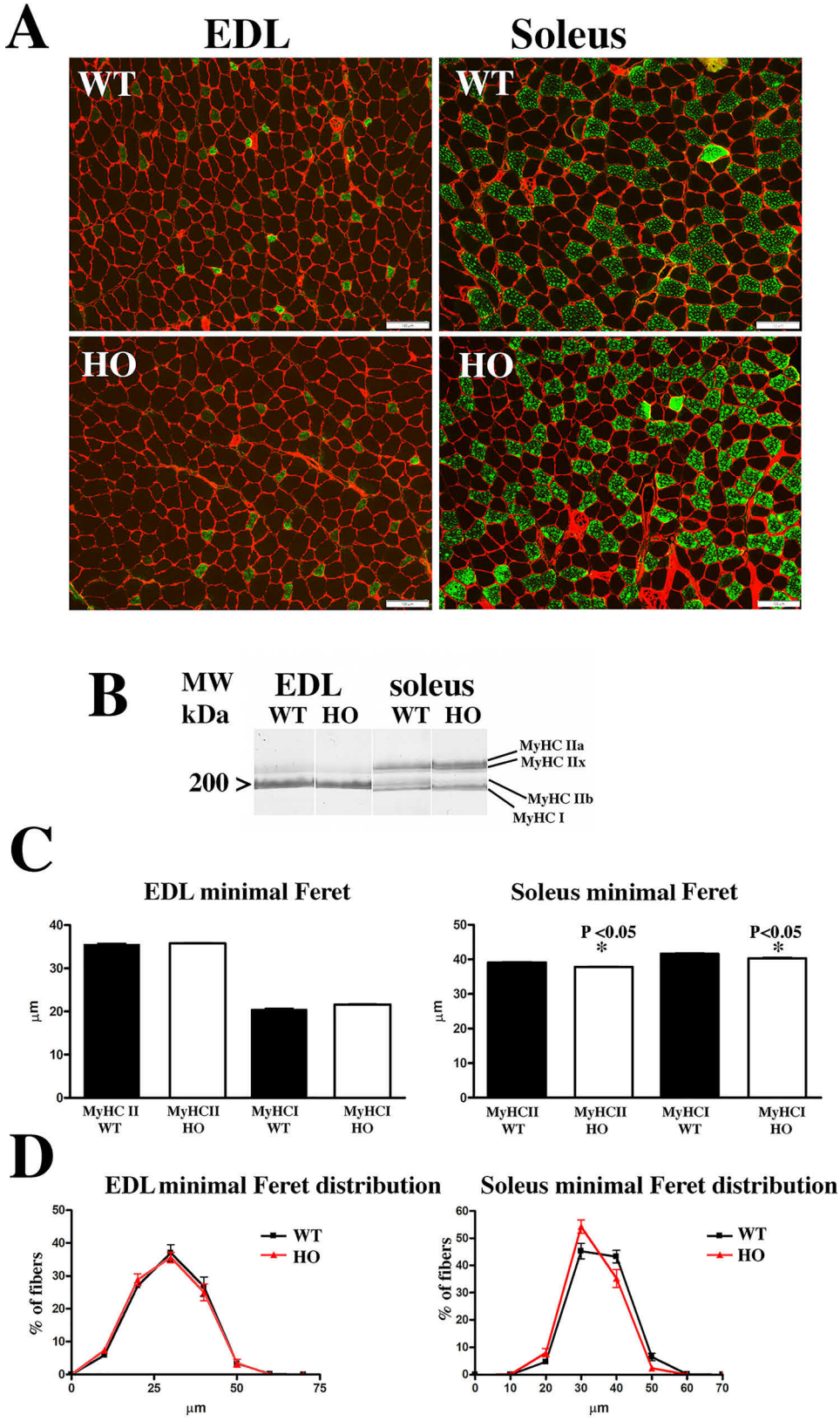

Figure 3. EDL and soleus muscles from HO91 mice do not show signs of atrophy or abnormal myosin heavy chain composition. *A*, EDL (*left*) and soleus (*right*) muscles were sectioned with a cryostat, stained with anti-laminin and anti-MyHC I Ab, imaged with an inverted fluorescent microscope, and analyzed as described in Experimental procedures. *HO*, homozygous. *Bar*, 200 μm. *B*, high-resolution SDS-PAGE and Coomassie brilliant blue staining of myosin heavy chain isoforms present in EDL and soleus muscles from WT and HO91 mice. No discernible difference in MyHC isoform expression was evident between the two genotypes. *C*, quantification of minimal Feret fiber size of EDL (*left*) and soleus (*right*) muscles from WT (*black bars*) and HO91 mice (*white bars*). Values are presented as mean (±S.E.). *D*, minimal Feret fiber distribution. Measurements were carried out on cross-sections of EDL (*left*) and soleus (*right*) muscles from WT (*black squares*, *continuous line*) and HO91 (*red triangles*, *continuous line*). WT soleus, 3740 fibers; HO91 soleus, 5200 fibers; WT EDL, 3699 fibers; HO91 EDL, 3753 fibers ($n = 2$ mice per genotype). Data points are expressed as mean (±S.E.). *, $p \leq 0.05$ by Dunnett's test.

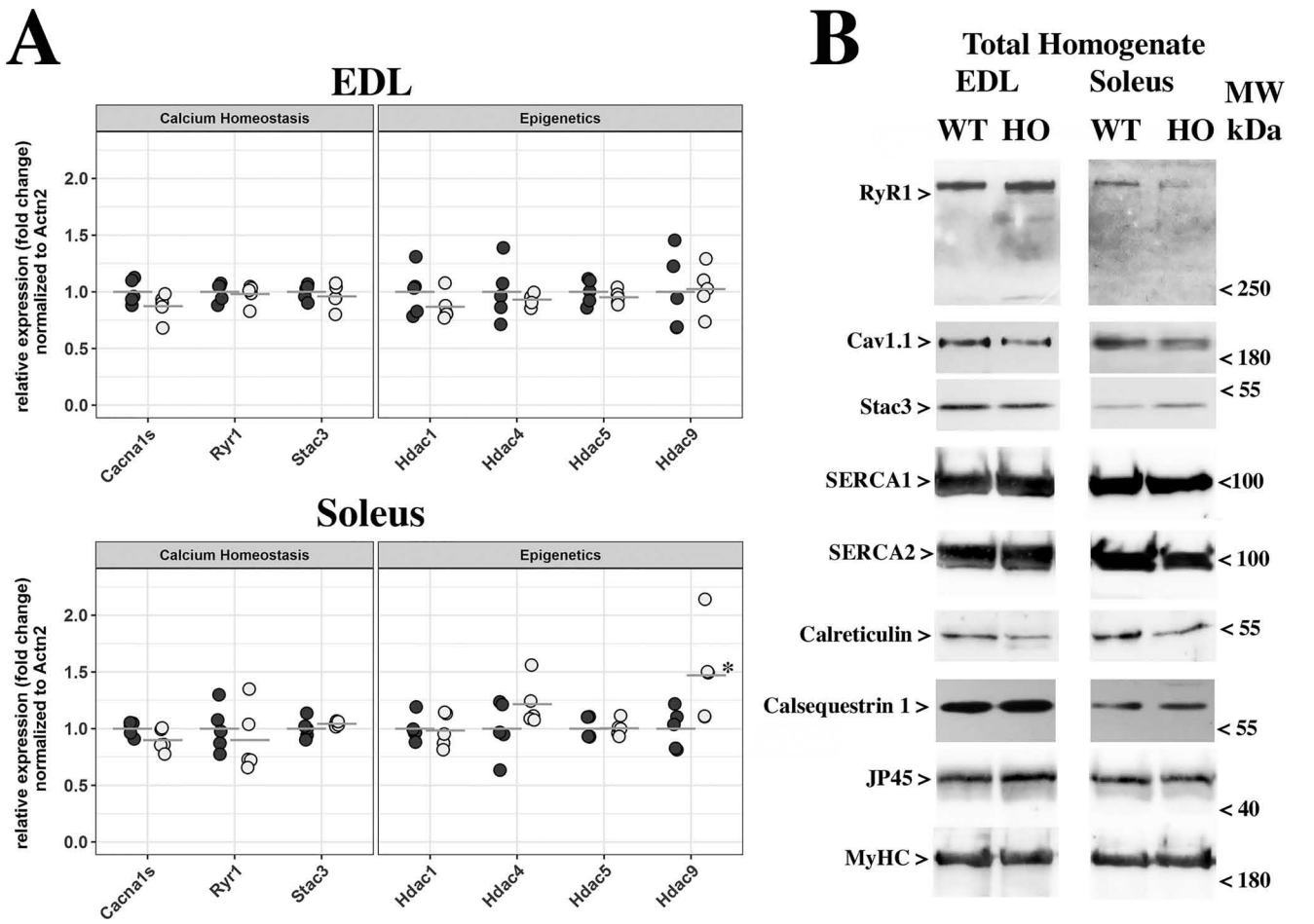

Figure 4. RyR1 protein and transcript levels are altered in soleus muscles from HO91 mice but not in EDL muscles. *A*, quantitative real-time PCR of the indicated transcripts in skeletal muscles from HO91 mice relative to WT littermates (the latter were set as 1). Transcript levels were normalized to Actn2 as a muscle-specific gene using the $\Delta\Delta C_T$ method. *, $p < 0.05$ (Student's *t* test). *B*, representative immunoblots of total homogenates of EDL and soleus muscles from WT and HO91 mice probed with the indicated antibodies.

it was 71.6 ± 6.6 nM (n = 24) and 68.2 ± 3.5 nM (n = 32) in WT and HO91 mice, respectively (Fig. 5*A*).

In the presence of 1.8 mM Ca^{2+} in the extracellular solution, the averaged peak Ca^{2+} transient induced by a single action potential in EDL fibers from WT mice was similar to that of HO91 mice (Fig. 5*B*). The mean (±S.D.) $\Delta F/F_0$ was 1.14 ± 0.52, n = 41, *versus* 1.17 ± 0.36, n = 50, respectively (Mann-Whitney test, $p > 0.05$). In contrast, the peak Ca^{2+} transients elicited in HO91 soleus fibers were decreased by 28% compared with those of the WT (Fig. 5*B*) (the mean ± S.D. $\Delta F/F_0$ was 0.51 ± 0.06, n = 39, *versus* 0.65 ± 0.09, n = 50, respectively; Mann-Whitney test, $p < 0.05$). No major changes in the kinetics of the Ca^{2+} transients were observed (Table S3). The summation of Ca^{2+} transient peaks evoked by a train of pulses delivered at 100 Hz in the presence of 1.8 mM Ca^{2+} in the extracellular solution in EDL fibers from HO91 mice was not different from that of WT mice (Fig. 5*B*) (the mean ± S.D. $\Delta F/F_0$ was 1.62 ± 0.38, n = 21, *versus* 1.64 ± 0.43, n = 23, respectively; Mann-Whitney test, $p > 0.05$) (Table S3). In soleus fibers from HO91 mice, the peak calcium transients induced by tetanic stimulation (Fig. 5*B*) was approximately 30% lower than that of WT mice (the mean ± S.D. $\Delta F/F_0$ was 1.12 ± 0.13, n = 24, *versus* 1.60 ± 0.11, respectively; Mann-Whitney test, $p <$ 0.05) (Table S3). Analysis of calcium homeostasis in *flexor digitorum brevis* (FDB) fibers from Het91 mice revealed no differences (i) in the resting $[Ca^{2+}]_i$, (ii) in the twitch Ca^{2+} transient, and (iii) in the Ca^{2+} transient elicited by tetanic stimulation between WT and Het91 mice (Fig. S4).

Discussion

Here, we investigated the skeletal muscle phenotype of a mouse model carrying the p.A4329D missense mutation in ex91 of the *Ryr1* gene. This study shows that the bi-allelic expression of the RyR1 p.A4329D mutation is phenotypically different from the mono-allelic expression of the same *Ryr1* mutation on the genetic background of a compound heterozygous carrier. In particular, the presence of the bi-allelic expression of the RyR1 p.A4329D mutation causes a mild muscle phenotype affecting mostly slow-twitch muscles, with minor, if any, effects on fast-twitch EDL muscles. Slow-twitch muscles from RyR1A4329D homozygous mice show a 60% reduction of RyR1 and $Ca_v1.1$ protein content and no changes in Stac3 content, whereas no changes were apparent in total homogenates of fast-twitch EDL muscles. The reduction of RyR1 content in slow-twitch muscles is accompanied by (i) a small reduction of minimal Ferret's diameter of soleus fibers and a 30% reduction

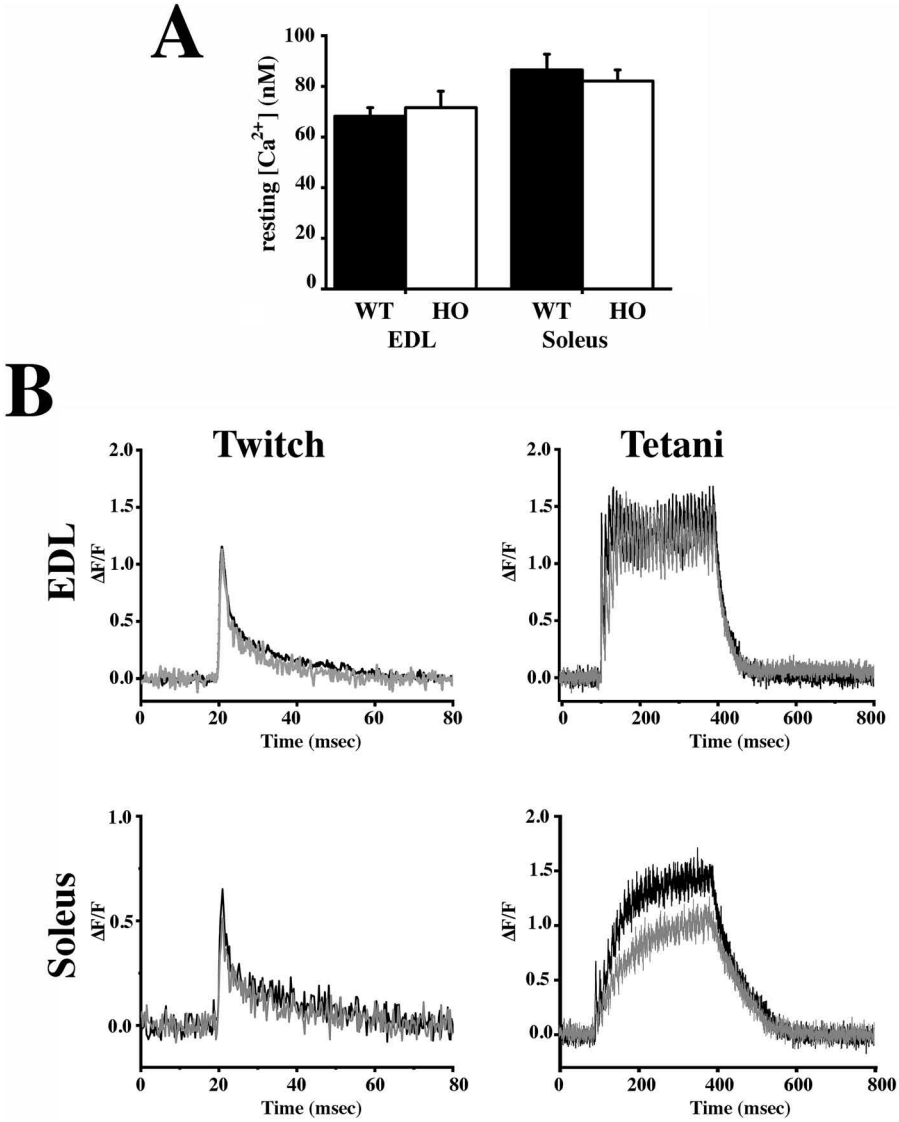

Figure 5. Electrically evoked peak Ca^{2+} transients are reduced in soleus muscles from HO91 mice but not in EDL muscles. *A*, mean (±S.E.) resting $[Ca^{2+}]_i$ measured in Fura-2-loaded EDL and soleus fibers. No difference was seen between controls (*black bars*) and HO91 (*white bars*). *B*, enzymatically dissociated EDL and soleus fibers were loaded with Mag-Fluo-4 and electrically stimulated by field stimulation. *Left*, representative Ca^{2+} transient elicited by a single pulse of 50 V, 1-ms duration. *Right*, representative Ca^{2+} transient elicited by a train of pulses delivered at 100 Hz for 300 ms. *Black trace*, WT; *gray trace*, HO91.

of (ii) peak twitch and tetanic force development and (iii) peak tetanic calcium transients.

Fiber type specificity of the muscle phenotype associated with the bi-allelic expression of the RyR1 p.A4329D mutation

The basic mechanism of ECC is similar between different fiber types; however, there are functional and structural heterogeneities within the calcium homeostasis toolkit between fast- and slow-twitch muscles controlling the kinetics of the calcium transients leading to muscle contraction (19). The ECC macromolecular complex of slow-twitch muscles shows distinct qualitative and quantitative features compared with those of fast-twitch muscles that might be important and account for the fiber type specificity of the muscle phenotype of the HO91 mice. Indeed, in slow-twitch muscles the membrane density of the DHPR and RyR1 is ~2- to 3-fold lower than that present in fast-twitch muscles (20–22), and we hypothesize that a further reduction in their content, below a critical level, impacts ECC, as seen in soleus muscles. As to the cause of the decreased RyR1 content in HO91 soleus muscles, it cannot be because of protein instability, as it would have occurred in all muscle types. In this context, it is interesting that the mechanical properties of extraocular muscles from HO91 mice were similar to those of WT littermates, as was the RyR1 protein level (23). The reduction in RyR1 and $Ca_v1.1$ may be caused at least in part by alterations of transcriptional regulation brought about by epigenetic modifications. Compatibly, in soleus muscles (but not in EDL muscles), HDAC9 levels were increased. HDAC9, like HDAC4, HDAC5, and HDAC7, is a member of the class II HDAC family (24), and these enzymes are involved in chromatin modification and regulation of mef-2-dependent transcription (25, 26). Furthermore, HDAC4 and HDAC5 levels are increased in the muscles of patients carrying recessive *RYR1* mutations (13).

Calcium-induced calcium release in mammalian skeletal muscles: fast-twitch versus slow-twitch muscles

The domain between rabbit RyR1 residues 4274 and 4535 is a regulatory domain (27). Additionally, we have shown that the RyR1 p.A4329D mutation decreases the sensitivity of RyR1 to calcium and caffeine (15). The A4329 residue is distant from the amino acid residues that have been proposed to come from the RyR1 calcium binding sites in the linear RyR1 sequence (28). High-resolution cryo-EM of RyR1 has shown that E3893, E3967, and T5001, plus amino acids H3895 and Q3970, make up the high-affinity calcium binding site, which is likely to be involved in calcium-dependent RyR1 activation. The resolution of the amino acid sequence encompassing residue A4329 of the available RyR1 3D structure is poor, and presently it is still not possible to establish exactly whether A4329 interacts with any of the above-mentioned key residues to destabilize the conformation of the calcium binding site. As to the mechanism by which the low-calcium and caffeine sensitivity of RyR1 p.A4329D channels contribute to the muscle phenotype of the HO91 mice, it may relate to transcriptional regulation. Indeed, it is possible that the downregulation of calcium-induced calcium release in slow-twitch fibers affects the activity of calcium-dependent transcription factors such as MEF2 and NFAT (18, 29), which, in turn, might be involved in the expression of RyR and Cav1.1 in muscles. Our results suggest that the calcium-dependent regulation of the RyR1 is relevant, at least in part, in determining the molecular and functional signature of slow-twitch muscles (30, 31) but have a negligible effect on the characteristics of fast-twitch muscles.

Bi-allelic expression of the RyR1 p.A4329D mutation versus mono-allelic expression of the RyR1 p.A4329D mutation on the genetic background of a compound heterozygous carrier

Comparison of compound heterozygous RyR1Q1970fsX16+A4329D mice with age-matched homozygous RyR1A4329D mice shows that the former exhibit a defect of postnatal body weight gain. The weight gain defects affect both male and female RyR1Q1970fsX16+A4329D double knock-in mice. In the present paper, we show that the bi-allelic expression of the single RyR1 p.A4329D mutation does not affect the body weight growth curve or the phenotype of fast-twitch muscles. Therefore, the impairment of the early postnatal development of the compound heterozygous RyR1Q1970fsX16+A4329D mice might affect the maturation of fast-twitch muscles, leading to a decrease of RyR1 expression and the appearance of a muscle phenotype in EDL muscles.

In conclusion, our data are consistent with the hypothesis that intracellular pathways that are activated by the bi-allelic expression of the RyR1 p.A4329D mutation are not identical to those activated by the mono-allelic expression in a compound heterozygous genetic background, and that such a divergence accounts for the diversity of the muscle phenotype of the mice carrying these recessive *RYR1* mutations.

Experimental procedures

Compliance with ethical standards

All experiments were carried out on 8–12-week-old male mice unless otherwise stated. All experimental procedures were approved by the Cantonal Veterinary Authority of Basel Stadt (BS Kantonales Veterinäramt permit numbers 1728 and 2115).

Genotyping RyR1A4329D mice and real-time qPCR

PCR amplification of *Ryr1* exon 91 was performed on genomic DNA of WT and HO91 mice using specifically designed primers (Table S1), as previously described (15). GoTaq® DNA polymerase (Promega) was used in the amplification of the product, as previously described (15). The amplified DNA products were digested with PvuII (R0151L BioLabs) for 1 h at 37 °C, separated on a 7.5% polyacrylamide gel, and stained with ethidium bromide to visualize DNA bands. For quantitative real-time PCR (qPCR), cDNA was prepared from total RNA extracted from frozen muscles using TRIzol® (ThermoFischer; 15596026) according to the manufacturer's instructions. DNA was removed using DNase I (Invitrogen; 18068-015), and 1000 ng RNA was reverse transcribed into cDNA using the high-capacity cDNA reverse transcription kit (Applied Biosystems; 4368814). The cDNA was amplified by qPCR using the primers listed in Table S1, and transcript levels were quantified using Power SYBR® Green reagent master mix (Applied Biosystems; 4367659), using the Applied Biosystems 7500 Fast real-time PCR system running 7500 software, version 2.3, as previously described (15). Transcript quantification was based on the comparative $\Delta\Delta C_T$ method. Each reaction was performed in duplicate, and results are expressed as relative gene expression normalized to that of actinin (Actn2).

In vivo muscle strength assessment

Mice were individually housed in cages equipped with a running wheel carrying a magnet, as previously described (15). Wheel revolutions were registered by reed sensors connected to an I-7053D digital-input module (Spectra), and the revolution counters were read by a standard laptop computer via an I-7520 RS-485-to-RS-232 interface converter (Spectra). Digitized signals were processed by the "mouse running" software developed at Santhera Pharmaceuticals. Total running distance (meters) and speed (km/h) were evaluated.

In vitro muscle strength assessment

To test muscle force *in vitro*, EDL and soleus muscles were dissected from 12-week-old mice and mounted onto a muscle force-transducing setup (Heidelberg Scientific Instruments), as previously described (15). Muscle force was digitized at 4 kHz by using an AD Instrument converter and stimulated with 15-V pulses for 1.0 ms. EDL tetanus was recorded in response to a train of pulses of 1.0-ms duration delivered at 50/100/150 Hz and 50/100/120 Hz for EDL and soleus muscle, respectively, for 400 ms and 1100 ms. Specific force was normalized to the muscle cross-sectional area [wet weight (mg)/length (mm) × 1.06 (density, mg/mm^3)].

Intracellular [Ca^{2+}] measurements

For resting [Ca^{2+}] measurements, single fibers were isolated from 6–7-week-old mice and plated on 35-mm glass-bottom dishes (MatTek Corp.) coated with 5 μl (1 mg/ml) of laminin (ThermoFischer), as previously described (15). The fibers were incubated for 20 min at 20 °C in normal mammalian Ringer's buffer (137 mM NaCl, 5.4 mM KCl, 0.5 mM $MgCl_2$, 1.8 mM $CaCl_2$, 0.1% glucose, 11.8 mM HEPES, pH 7.4, NaOH) containing 5 μM Fura-2, AM (Invitrogen). The excess Fura-2 was diluted out by the addition of fresh Ringer's solution, and measurements of the resting [Ca^{2+}] were carried out as previously described (13, 15), using an inverted Zeiss Axiovert fluorescent microscope. Only those fibers that contracted when an electrical stimulus was applied were used for the [Ca^{2+}] measurements.

For electrically evoked Ca^{2+} transients, single fibers were incubated for 10 min at 19 °C in Ringer's solution containing 10 μM low-affinity calcium indicator Mag-Fluo-4 AM (ThermoFischer), 50 μM *N*-benzyl-*p*-toluene sulfonamide (BTS, Tocris). Fibers were rinsed twice with fresh Tyrode's solution, and measurements were carried out in Tyrode's solution containing 50 μM BTS as previously described (15). Measurements were carried out with a Nikon Eclipse inverted fluorescent microscope equipped with a 20× PH1 DL magnification objective. The light signals from a spot of 1-mm diameter of the magnified image of single fibers were converted into electrical signals by a photomultiplier from Myotronic (Heidelberg, Germany) connected to a PowerLab Chart 5 analog digital interface. Fluorescent signals were analyzed using PowerLab Chart 5 and Origin 6.0 software. Changes in fluorescence were calculated as $\Delta F/F_0 = (F_{max} - F_{rest})/(F_{rest})$. Kinetic parameters were analyzed using PowerLab Chart5 software. Fibers were excited at 480 nm and then stimulated with a single pulse of 50 V of 1-ms duration or with a train of pulses of 50 V of 1-ms duration delivered at 100 Hz for 300 ms. Fibers were isolated from 3–5 mice, and the results were pooled.

Histological examination

Muscles from WT and HO91 mice were isolated and mounted for fluorescence microscopy imaging. Changes in muscle fiber type and calculation of the minimal Feret diameter, the closest possible distance between the two parallel tangents of an object, were determined as described previously (32). Images were obtained using an Olympus IX series microscope and analyzed using CellP software.

Biochemical analysis of total muscle homogenates

Total muscle homogenates were prepared from EDL and soleus muscles of WT and HO91 mice. SDS-PAGE and Western blotting of total homogenates were carried out as previously described (13, 15). Western blots were stained with the primary antibodies listed in Table S2, followed by peroxidase-conjugated protein G (Sigma, P8170; 1:130,000) or peroxidase-conjugated anti-mouse IgG (Fab-specific) antibody (Sigma, A2304; 1:200,000). The immunopositive bands were visualized by chemiluminescence using the WesternBright ECL-HRP substrate (Witec AG). Densitometry of the immune-positive bands was carried out using Fusion Solo S (Witec AG). A representative immunoblot of each antibody on total muscle homogenates from WT mice is shown in Fig. S3.

Statistical analysis

Statistical analysis was performed using Student's unpaired *t* test for normally distributed values and the Mann-Whitney *U* test when values were not normally distributed. A p value of <0.05 was considered significant.

Data availability

All data are contained within the manuscript.

Acknowledgments—We thank Anne-Sylvie Monnet for technical support. The support of the Department of Anesthesia Basel University Hospital is gratefully acknowledged.

Author contributions—M. E., A. R., C. T., C. B., S. N., J. E., and S. B. designed and performed the experiments, characterized the mouse lines, and analyzed the results, with guidance from F. Z. and S. T.; P. P. created the mouse lines; M. E. and A. R. helped; F. Z. and S. T. designed the experiments on the mouse model, oversaw the project, and wrote the paper; all authors reviewed and helped elaborate on the manuscript.

Funding and additional information—This work was supported by Grants SNF 31003A-169316 and SNF 310030-184765 from the Swiss National Science Foundation, a grant from the Swiss muscle foundation (FSRMM), a grant from NeRAB, Botnar Stiftung (OOG-19-001), and PRIN 2015 to F. Z.

Conflict of interest—The authors declare that they have no conflicts of interest with the contents of this article.

Abbreviations—The abbreviations used are: CCD central core disease; CNM, centronuclear myopathy; DHPR, dihydropyridine receptor; DNMT, DNA methyltransferase; ECC, excitation contraction coupling; EDL, *extensor digitorum longus*; FDB, *flexor digitorum brevis*; HDAC, histone deacetylase; HO91, homozygous RyRA3249D mouse; Het91, homozygous RyRA3249D mouse; MmD, multi-minicore disease; MyHC, myosin heavy chain; RyR, ryanodine receptor; SR, sarcoplasmic reticulum; SERCA, sarco (endo)plasmic CaATPase; qPCR, real-time quantitative PCR.

References

1. Melzer, W., Herrmann-Frank, A., and Luttgau, H. C. (1995) The role of Ca^{2+} ions in excitation-contraction coupling of skeletal muscle fibres. *Biochim. Biophys. Acta* **1241,** 59–116 CrossRef Medline
2. Rios, E., and Pizarro, G. (1991) Voltage sensor of excitation-contraction coupling in skeletal muscle. *Physiol. Rev.* **71,** 849–908 CrossRef Medline
3. Franzini-Armstrong, C., and Protasi, F. (1997) Ryanodine receptors of striated muscles: a complex channel capable of multiple interactions. *Physiol. Rev.* **77,** 699–729 CrossRef Medline
4. Meissner, G. (2017) The structural basis of ryanodine receptor ion channel function. *J. Gen. Physiol.* **149,** 1065–1089 CrossRef Medline
5. Franzini-Armstrong, C., and Jorgensen, A. O. (1994) Structure and development of E-C coupling units in skeletal muscle. *Annu. Rev. Physiol.* **56,** 509–534 CrossRef Medline

6. Jungbluth, H., Treves, S., Zorzato, F., Sarkozy, A., Ochala, J., Sewry, C., Phadke, R., Gautel, M., and Muntoni, F. (2018) Congenital myopathies: disorders of excitation-contraction coupling and muscle contraction. *Nat. Rev. Neurol.* **14,** 151–167 CrossRef Medline
7. Treves, S., Jungbluth, H., Muntoni, F., and Zorzato, F. (2008) Congenital muscle disorders with cores: the ryanodine receptor calcium channel paradigm. *Curr. Opin. Pharmacol.* **8,** 319–326 CrossRef Medline
8. Zhou, H., Jungbluth, H., Sewry, C. A., Feng, L., Bertini, E., Bushby, K., Straub, V., Roper, H., Rose, M. R., Brockington, M., Kinali, M., Manzur, A., Robb, S., Appleton, R., Messina, S., *et al.* (2007) Molecular mechanisms and phenotypic variation in RYR1-related congenital myopathies. *Brain* **130,** 2024–2036 CrossRef Medline
9. Robinson, R., Carpenter, D., Shaw, M. A., Halsall, J., and Hopkins, P. (2006) Mutations in RYR1 in malignant hyperthermia and central core disease. *Hum. Mutat.* **27,** 977–989 CrossRef Medline
10. Wilmshurst, J. M., Lillis, S., Zhou, H., Pillay, K., Henderson, H., Kress, W., Müller, C. R., Ndondo, A., Cloke, V., Cullup, T., Bertini, E., Boennemann, C., Straub, V., Quinlivan, R., Dowling, J. J., *et al.* (2010) RYR1 mutations are a common cause of congenital myopathies with central nuclei. *Ann. Neurol.* **68,** 717–726 CrossRef Medline
11. Monnier, N., Marty, I., Faure, J., Castiglioni, C., Desnuelle, C., Sacconi, S., Estournet, B., Ferreiro, A., Romero, N., Laquerriere, A., Lazaro, L., Martin, J.-J., Morava, E., Rossi, A., Van der Kooi, A., *et al.* (2008) Null mutations causing depletion of the type 1 ryanodine receptor (RYR1) are commonly associated with recessive structural congenital myopathies. *Hum. Mutat.* **29,** 670–678 CrossRef Medline
12. Clarke, N. F., Waddell, L. B., Cooper, S. T., Perry, M., Smith, R. L., Kornberg, A. J., Muntoni, F., Lillis, S., Straub, V., Bushby, K., Guglieri, M., King, M. D., Farrell, M. A., Marty, I., Lunardi, J., *et al.* (2010) Recessive mutations in RYR1 are a common cause if congenital fiber type disproportion. *Hum. Mutat.* **31,** E1544–E1550 CrossRef Medline
13. Rokach, O., Sekulic-Jablanovic, M., Voermans, N., Wilmshurst, J., Pillay, K., Heytens, L., Zhou, H., Muntoni, F., Gautel, M., Nevo, Y., Mitrani-Rosenbaum, S., Attali, R., Finotti, A., Gambari, R., Mosca, B., *et al.* (2015) Epigenetic changes as a common trigger of muscle weakness in congenital myopathies. *Hum. Mol. Genet.* **24,** 4636–4647 CrossRef Medline
14. Klein, A., Lillis, S., Munteanu, I., Scoto, M., Zhou, H., Quinlivan, R., Straub, V., Manzur, A. Y., Roper, H., Jeannet, P. Y., Rakowicz, W., Jones, D. H., Jensen, U. B., Wraige, E., Trump, N., *et al.* (2012) Clinical and genetic findings in a large cohort of patients with ryanodine receptor 1 gene-associated myopathies. *Hum. Mutat.* **33,** 981–988 CrossRef Medline
15. Elbaz, M., Ruiz, A., Bachmann, C., Eckhardt, J., Pelczar, P., Venturi, E., Lindsay, C., Wilson, A. D., Alhussni, A., Humberstone, T., Pietrangelo, L., Boncompagni, S., Sitsapesan, R., Treves, S., and Zorzato, F. (2019) Quantitative RyR1 reduction and loss of calcium sensitivity of RyR1Q1970fsX16+A4329D cause cores and loss of muscle strength. *Hum. Mol. Genet.* **28,** 2987–2999 CrossRef Medline
16. Mosca, B., Delbono, O., Laura Messi, M., Bergamelli, L., Wang, Z.-M., Vukcevic, M., Lopez, R., Treves, S., Nishi, M., Takeshima, H., Paolini, C., Martini, M., Rispoli, G., Protasi, F., and Zorzato, F. (2013) Enhanced dihydropyridine receptor calcium channel activity restores muscle strength in JP45/CASQ1 double knockout mice. *Nat. Commun.* **4,** 1541 CrossRef Medline
17. Treves, S., Vukcevic, M., Maj, M., Thurnheer, R., Mosca, B., and Zorzato, F. (2009) Minor sarcoplasmic reticulum membrane components that modulate excitation-contraction coupling in striated muscles. *J. Physiol.* **587,** 3071–3079 CrossRef Medline
18. Schulz, R. A., and Yutzey, K. E. (2004) Calcineurin signalling and NFAT activation in cardiovascular and skeletal muscle development. *Dev. Biol.* **266,** 1–16 CrossRef Medline
19. Baylor, S. M., and Hollingworth, S. (2012) Intracellular calcium movements during excitation-contraction coupling in mammalian slow-twitch and fast-twitch muscle fibers. *J. Gen. Physiol.* **139,** 261–272 CrossRef Medline
20. Lamb, G. D. (1992) DHP receptors and excitation-contraction coupling. *J. Muscle Res. Cell Motil.* **13,** 394–405 CrossRef Medline
21. Bers, D. M., and Stiffel, V. M. (1993) Ratio of ryanodine to dihydropyridine receptors in cardiac and skeletal muscle and implications for E-C coupling. *Am. J. Physiol.* **264,** C1587–C1593 CrossRef
22. Anderson, K., Cohn, A. H., and Meissner, G. (1994) High-affinity [^{3}H] PN200-l 10 and [^{3}H] ryanodine binding to rabbit and frog skeletal muscle. *Am. J. Physiol.* **266,** C462–C466 CrossRef
23. Eckhardt, J., Bachmann, C., Benucci, S., Elbaz, M., Ruiz, A., Zorzato, F., and Treves, S. (2020) Molecular basis of impaired extraocular muscle function in a mouse model of congenital myopathy due to compound heterozygous *Ryr1* mutations. *Hum. Mol. Genet.* **29,** 1330–1339 CrossRef
24. Haberland, M., Montgomery, R. L., and Olson, E. N. (2009) The many roles of histone de-acetylases in development and physiology: implications for disease and therapy. *Nat. Rev. Genet.* **10,** 32–42 CrossRef Medline
25. Potthoff, M. J., Wu, H., Arnold, M. A., Shelton, J. M., Backs, J., McAnally, J., Richardson, J. A., Bassel-Duby, R., and Olson, E. N. (2007) Histone deacetylase degradation and MEF2 activation promote the formation of slow-twitch myofibers. *J. Clin. Invest.* **117,** 2459–2467 CrossRef
26. Han, A., He, J., Wu, Y., Liu, J. O., and Chen, L. (2005) Mechanism of recruitment of class II histone deacetylases by myocyte enhancer factor-2. *J. Mol. Biol.* **345,** 91–102 CrossRef Medline
27. Du, G. G., Avila, A., Sharma, P., Khanna, V. K., Dirksen, R. T., and MacLennan, D. H. (2004) Role of the sequence surrounding predicted transmembrane helix M4 in membrane association and function of the Ca^{2+} release channel of skeletal muscle sarcoplasmic reticulum (Ryanodine Receptor Isoform 1). *J. Biol. Chem.* **279,** 37566–37574 CrossRef Medline
28. Des Georges, A., Clarke, O. B., Zalk, R., Yuan, Q., Condon, K. J., Grassucci, R. A., Hendrickson, W. A., Marks, A. R., and Frank, J. (2016) Structural basis for gating and activation of RyR1. *Cell* **167,** 145–157 CrossRef Medline
29. Bassel-Duby, R., and Olson, E. (2006) Signaling pathways in skeletal muscle remodeling. *Annu. Rev. Biochem.* **75,** 19–37 CrossRef Medline
30. Salviati, G., and Volpe, P. (1988) Ca^{2+} release from sarcoplasmic reticulum of skinned fast- and slow-twitch muscle fibers. *Am. J. Physiol.* **254,** C459–C465 CrossRef Medline
31. Isaacson, A., Hinkes, M. J., and Taylor, S. R. (1970) Contractile and twitch potentiation of fast and slow muscles of the rat at 20 and 37 C. *Am. J. Physiol.* **218,** 33–41 CrossRef Medline
32. Briguet, A., Courdier-Fruh, I., Foster, M., Meier, T., and Magyar, J. P. (2004) Histological parameters for the quantitative assessment of muscular dystrophy in the mdx-mouse. *Neuromuscul. Disord.* **14,** 675–682 CrossRef Medline